A Textile Architecture-Based Discrete Modeling Approach for Fabric Draping Simulations

QINGXUAN WEI1 and DIANYUN ZHANG1,*

ABSTRACT

Adoption of lightweight composites for structural components is transforming the transportation industry in pursuit of improved performance and better fuel economy. In Liquid Composite Molding (LCM), dry fabric deformation in the draping process gains lots of attention as it affects the fiber orientation, leading to variations in fabric permeability and the resulting final quality of the product due to the change in infusion and curing processes. The lack of robust modeling tools makes the composite manufacturers heavily reliant on trial-and-error approaches to minimize part variability, resulting in high manufacturing costs and limiting innovations for new process and part designs. The current study develops a modeling approach to predict the deformation for dry fabric. In the model, fabric is made of interlacing virtual fiber tows which are represented by Timoshenko beams joint by translational and rotational springs. Dashpots at intersections are used to capture energy dissipation. The proposed model features the simplicity and efficiency in the prediction of shear angle when fabric is subject to 3-dimensional loading. Another highlight of this study is the consideration of characterized relaxation behavior of fabric subject to in-plane shear loading. Cantilever beam bending tests and picture frame tests were carried out to characterize material properties, geometric characteristics, spring stiffness, and damping coefficients. The proposed model was applied to a hemisphere draping model implemented in Abaqus to demonstrate the predictive capability.

Keywords: discrete model, shear angle, bending behavior, draping simulation

¹School of Aeronautics and Astronautics, Purdue University, 701 W Stadium Ave, West Lafayette, IN 47907-2045, USA

^{*}Corresponding Author(s)

INTRODUCTION

Manufacturing of lightweight composites involves complex deformation of fibers that inevitably causes part variability and unintended defects, such as fiber wrinkles, voids, residual stresses, and geometric distortions [1–15]. In Liquid Composite Molding (LCM), flat dry fabrics are draped onto a mold with complex geometries, which can affect the subsequent infusion process and induce fabric wrinkling [16]. Predicting fabric deformation with robust modeling tools makes fabric wrinkle reduction less reliant on trial-and-error approaches, saving manufacturing costs and improving part design.

The state-of-the-art simulation approaches for fabric deformation can be divided into three main categories: (1) continuum mechanics-based models, (2) semi-discrete models, and (3) discrete models. Continuum mechanics-based models treat textile fabric as a piece of continuous material which is homogenized by Unit Cells (UC) [17–21]. Hyperelastic and hypoelastic constitutive models are commonly adopted for UC since fabrics usually undergo large deformation. Semi-discrete models incorporate the yarn structures into a user-defined finite element in a Finite Element Modeling (FEM) setting. Different deformation modes are considered to derive internal nodal loads [22–24]. Even though continuous and semi-discrete models can predict fabric deformation accurately, they do not provide intuitive images of yarn deformation and promote the understanding of the mechanics of yarn deformation when fabric is subject to complex loading. Instead, they are based on the analysis in which yarn deformation cannot be directly seen. Therefore, an efficient and robust discrete model is necessary.

In discrete models, fabric architecture is modeled explicitly. Commonly a textile fabric is decomposed into woven cells consisting of individual yarns. Digital fiber approach even breaks each yarn into a bundle of digital fibers made of cylinder bars connected by frictionless pin-joints [25,26]. Larger number of fibers per yarn can increase the modeling accuracy. The approach is able to capture inter-yarn and intrayarn deformation. There are also many studies in which a fiber yarn is continuous. Typically, the continuous yarns are treated as orthotropic solid material with circular, ellipse, or lenticular cross-sections [27–29]. Inter-yarn behavior is modeled through a master-slave contact and Coulomb friction. The complex yarn geometry brings vast degrees of freedom and result in high computational costs especially for a large modeling domain. To simplify the yarn geometry, Gatouillat et al. replaced the curve solid yarn with an artificial hypoelastic shell structure [30]. Each tow was modelled as a series of several flat shells, whose geometric parameters and material properties were characterized by uniaxial tension, bending, and picture frame tests. The penalty method and Coulomb law with a friction coefficient of 0.3 were the properties of contact pairs assigned at intersection area. Fiber tows can be further simplified into beam structures. Faccio Júnior simulated the plain-weave fabrics by constructing all the warp and weft varns as beams with wavy mid-surfaces [31]. Isotropic material properties were used and bending stiffness was multiplied by a reduction factor. Contact pairs and the pointwise contact constitutive law were utilized to describe the contact behavior. Saito and Neto also used beam elements to model warp and weft yarns [32]. The Rayleigh damping rather than friction was adopted in the study to consider energy dissipation. However, a large number of contact pairs used in the above-mentioned studies could lead to high computational costs and possible convergence issues. Harrison's model utilized hinge elements at the intersection of beams [33]. Sun and Pan regarded the

contact points at the intersection as welded joints and used cantilever beams to represent fiber tows [34]. Even though energy dissipation was considered in the previous studies, there is no study to characterize the relaxation behavior of fabric itself during in-plane shear deformation, yet the relaxation has been clearly observed in experiments.

This paper puts forward a discrete textile architecture-based model for woven fabrics. In the proposed approach, a sheet of fabric consists of interwoven virtual fiber tows modeled by Timoshenko beams. The contacts between fiber tows are modeled using translational and rotational springs at the joint of the beams. Energy dissipates through a dashpot rather than friction at the contact surface. The material properties were characterized by cantilever bending and picture frame tests. The model was validated by conducting hemisphere draping tests. It is expected that the proposed approach can be applied to various types of weave patterns without drastically changing the configuration since the weave is not created explicitly. Due to the simple yarn geometry and inter-yarn connections, the model is able to predict the fabric deformation efficiently and show a clear view of the yarn deformation.

The first part in this paper shows the modeling strategy including the geometry and materials along with the parameters to be characterized. The second section shows the characterization of geometric and material parameters through cantilever bending and picture frame tests. Finally, the modeling approach is applied to a hemisphere draping example to demonstrate the predictive capability.

MODELING APPROACH

In this section, the modeling strategy is elaborated with a focus on the in-plane shear behavior of a textile fabric. The constitutive model of each fiber tow is provided and the required parameters that should be experimentally characterized are summarized.

Model description

In the present paper, a piece of fabric is made of interlacing virtual fiber tows, modeled by beam structures. The in-plane bending behavior of yarn is relatively harder than out-of-plane bending behavior because in-plane bending is hindered by adjacent yarns in a single ply of fabric. To incorporate this effect, a rectangular cross-section was adopted so that the bending stiffness within the plane and out of the plane could be mainly controlled by b and a, respectively, as shown in Figure 1. Since the virtual fibers are straight and in the same plane, the model can be applied to multiple types of weave patterns without fully reconstructing the model. Different from Euler-Bernoulli beams, Timoshenko beams allow for shearing strain (i.e., the rotation of the cross-section does not equal to that of mid-surface). Therefore, the Timoshenko beam theory is more suitable for the present model because the shear strain within each tow represents intratow shear, which is a mechanism observed in the experiment. Rotational and translational springs are added at each intersection of the virtual fiber tows. The translational spring just connects the virtual fiber tows to avoid their separation, therefore, a linear spring is sufficient. The rotational spring controls the change of inplane shear angle. The nonlinear characteristic of in-plane shear behavior requires a highly nonlinear spring. The stiffness of the spring is defined as

$$k = \frac{dF}{dx} \tag{1}$$

where F is the force or moment, and x is the relative displacement or rotation angle. The energy dissipates through dashpots at the intersections. The damping coefficient is defined as

$$d = \frac{dF}{dv} \tag{2}$$

where v is the relative velocity $(v = \dot{x})$.

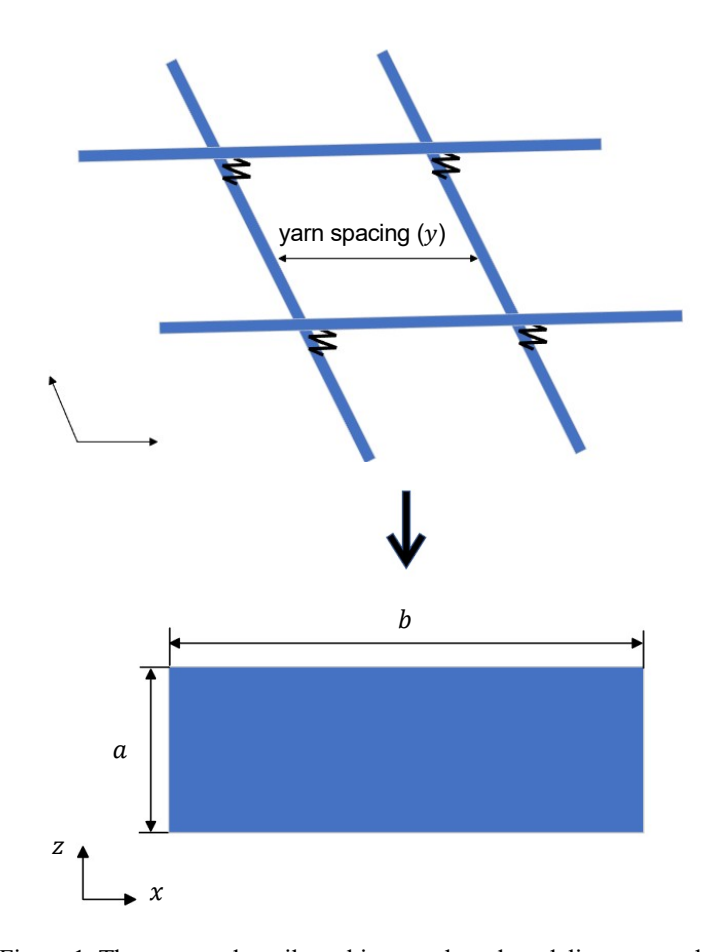


Figure 1. The proposed textile architecture-based modeling approach.

Nonlinear in-plane shear deformation

In order to set the rotational spring correctly, it is crucial to understand the in-plane shear behavior. A typical shear force vs. shear angle relation is shown in Figure 2 when a layer of fabric is subject to in-plane shear loading. Shear angle is an important parameter that describes the shear behavior which is commonly defined as the change of the angle between warp and weft yarns [29,34–43]. At the initial stage of in-plane shear, as the inter-yarn friction is overcome, it is generally believed that the rotation of

warp and weft yarns dominates the deformation mode. The space between fiber tows is gradually decreasing and the fiber bundles become closer to each other. Fiber sliding might also happen. No lateral compaction exists at this stage. The negligible shear force is mainly caused by friction between the yarns which is affected by the normal pressure exerted at the intersection [29,34–38,41]. Experiments conducted by Taha et al. show that the shear force at this stage does not differ a lot for various kind of fabrics [35]. With the fiber tows further rotating, the contact force grows even before lateral compaction, resulting in the increase of effective shear modulus of fabric [29]. As shear deformation further increases, fiber rotation is limited, and the fiber tows are compressed against each other at the side. Once the compressive load is too large, the out-of-plane wrinkling will happen as a result of buckling of fibers. The onset of wrinkling is shearing locking and the locking angle is the shearing angle at the locking point [36,40,43]. Transverse compression dominates the drastically increased shear force as the shear angle further increases. To match the nonlinear shear force, the stiffness of the rotational spring also needs to be nonlinear.

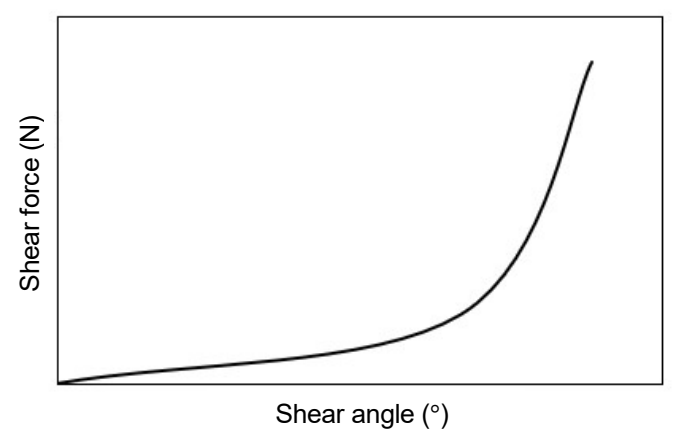


Figure 2. Shear force vs. shear angle for in-plane shear behavior.

Constitutive model of a virtual fiber

Since virtual fiber undergoes large deformation during draping process, a hyperelastic model should be adopted. In this paper, isotropic Neo-Hookean model was used to describe the constitutive law of virtual fiber tow. The strain energy density function is

$$W = C_1(\overline{I_1} - 3) + D_1(J - 1)^2 \tag{3}$$

An anisotropic model was not required due to that deformation mode remains the same with sufficiently large in-plane shear modulus and longitudinal modulus of the fiber tow. The results are not influenced by changing from an anisotropic constitutive model to an isotropic constitutive model. In total, there are six parameters to be characterized as listed in Table I. Note that they are only for virtual fiber tows and are not the same as those of real fiber tows.

TABLE I. PARAMETERS OF THE PROPOSED MODEL.

Parameters	Meaning			
а	Cross-section dimension in the out-of-plane direction			
b	Cross-section dimension in the in-plane direction			
ρ	Density of the fiber tow			
C_1	Parameter of the Neo-Hookean model			
D_1	Parameter of the Neo-Hookean model			
y	Yarn spacing			

PARAMETER CHARACTERIZATION

The characterization of material properties of T300 carbon fiber plain weave fabric is shown in this section. The bending properties were obtained through cantilever beam bending tests, and the in-plane shearing properties were characterized by conducting picture frame tests.

Bending behavior

Four specimens of 18" long and 3" wide were prepared. White lines were marked at 3", 6", and 9" away from one end as shown in Figure 3 (a). The region to the left of the mark was clamped between two metal blocks and the right part was suspended. So, the hanging length is 3", 6", and 9" and each length was tested four times. Average deflection was recorded by a camera as indicated in Figure 3 (b).

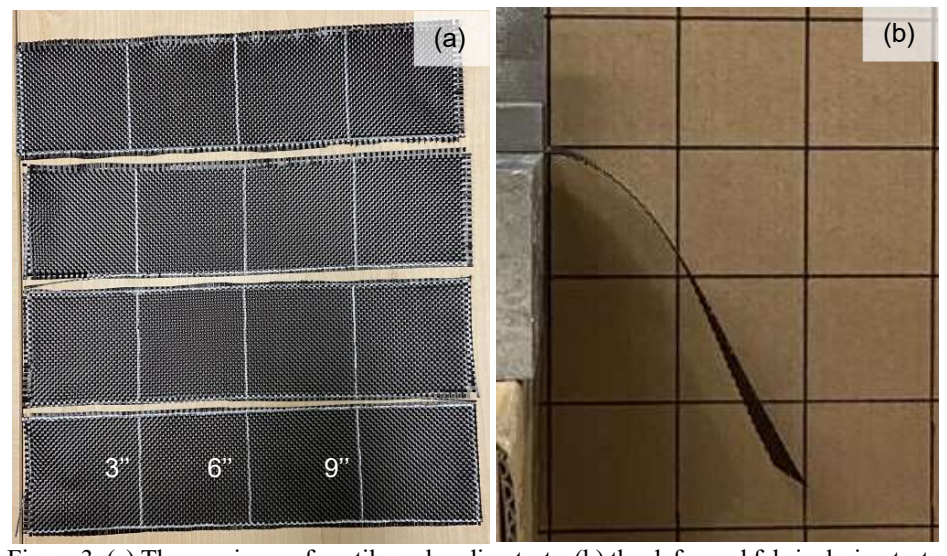


Figure 3. (a) The specimen of cantilever bending tests; (b) the deformed fabric during tests.

A corresponding bending model was built in Abaqus (in Figure 4 (a)). The fabric in the model consists of many virtual fibers which were modelled by Timoshenko beams. The left end of the fabric was fixed. To characterize the bending properties, the weight of the model should equal to the weight of the real fabric m. The weight of model was computed from cross-section dimensions a and b, length of virtual fiber tow along the warp direction l_1 and the weft direction l_2 , the number of warp tows n_1 and the number

of weft tows n_2 . Weight of real fabric is the product of the area A and the weight per area which is 0.21894 kg/m^2 as measured in experiments.

$$ab\rho(l_1n_1 + l_2n_2) = m (4)$$

The deformed shapes obtained from the simulation and the experiment are shown in Figure 4 (b).

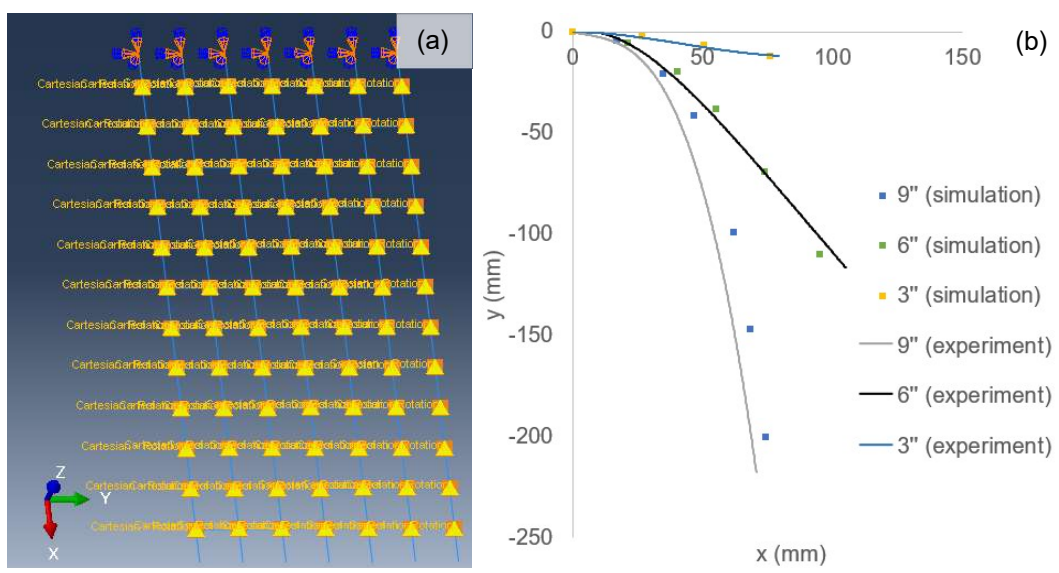


Figure 4. (a) The configuration of the proposed discrete model; (b) the deflections from the experiments and simulations.

In-plane shear behavior

Parameters cannot be fully characterized only by bending test. The behavior of fabric under in-plane shear was studied by picture frame tests and the corresponding numerical model.

PICTURE FRAME TEST

In the picture frame test, a piece of carbon fabric with materials cut at the corners was clamped by a set of metal frame (in Figure 5 (a)). The frame was mounted on an MTS tensile machine. The bottom crosshead first moved downwards at 35 mm/min for 96 mm. Then, it stayed still for 3 minutes and finally moved back at 35 mm/min to the initial position. Force, time and displacement were recorded, and the initial force and displacement were both set to zero. Shear angle γ illustrated in Figure 5 (b) can be computed from displacement according to the following expressions:

$$\gamma = \frac{\pi}{2} - 2\theta \tag{5}$$

$$\gamma = a\cos(\frac{\sqrt{2}L_{frame} + d}{2L_{frame}}) \tag{6}$$

where L_{frame} is the length of frame and d is the displacement of the crosshead. The normalized shear force $F_{normalized}$ is related to the measured force $F_{measured}$ and a half of the angle between the weft and warp tows θ [42]. The calculation excludes the effect of frame size and fabric size and makes the results more representative for T300 carbon fiber reinforced plain weave fabric [44].

$$F_{normalized} = F_{shear} \times \frac{L_{frame}}{L_{fabric}^2} \tag{7}$$

$$F_{shear} = \frac{F_{measured}}{2\cos\theta} \tag{8}$$

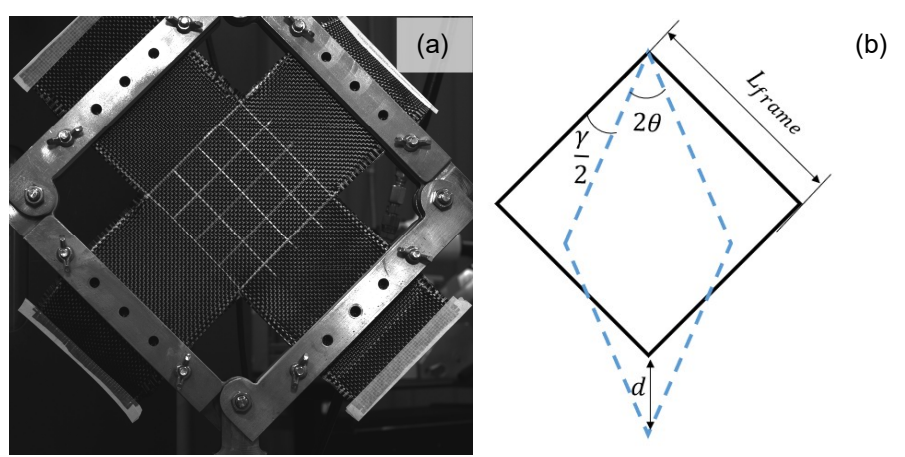


Figure 5. (a) The setup of picture frame test; (b) Illustration of the movement of the picture frame.

The normalized shear force vs. shear angle obtained from the test is shown in Figure 6 together with the deformed shape of the fabric. Initially, the normalized shear force is very small and there are large channels between fiber tows. As the channels gradually close, the force increases almost linearly with shear angle. Then, the shear force suddenly increases around shear locking point due to compaction of neighboring yarns. After locking, shear force increases linearly again with an increased shear angle but with large stiffness. Wrinkles can be observed during this stage. The normalized shear force is also plotted against time in Figure 7 to show the viscous behavior of fabric. Once the crosshead stops to move, the normalized shear force decreases from the maxima first greatly within a few seconds. Then, the force steadily decreases with small rate till the return of the crosshead.

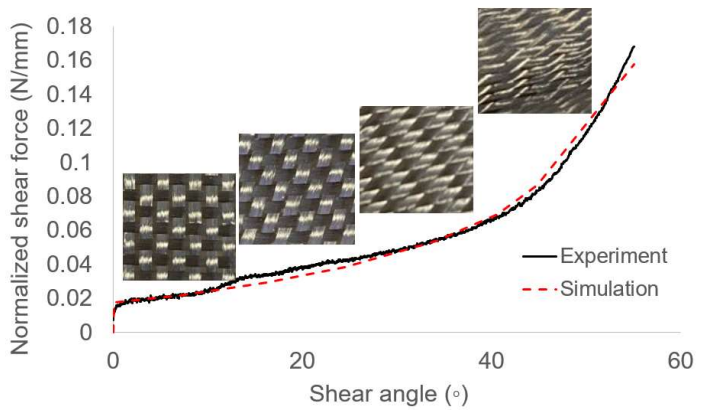


Figure 6. The shear force vs. shear angle responses obtained from the experiment and simulation.

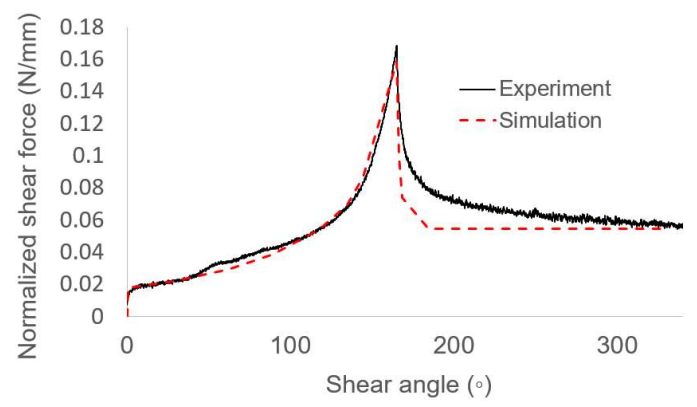


Figure 7. The normalized shear force vs. time responses obtained from the experiment and simulation.

IN-PLANE SHEAR MODEL

An FEM model for the picture frame test was built in Abaqus. Fibers were created as wire parts meshed by 2-node linear beams in space (B31). The beam section was integrated during the analysis. Frames were modelled as isotropic beams with linear elastic material properties and circular cross-sections. The modulus of the frame bar was set to 10^7 MPa which is much larger than the modulus of fiber. The ends of frame bars were pinned together. The virtual fibers were also pinned to the frame. Relative rotation at each pin-joint was allowed. The bottom left corner of the frame was fixed, and top right corner was moved at 35 mm/min (the same as the speed in experiment) at 45° with respect to the *x*-axis for 2.62 minutes. The length of frame L_{frame} is 192mm, and the length of fabric at the center L_{fabric} is 96mm. The dimensions are not required to equal to those in the real experiment, as the shear force is normalized.

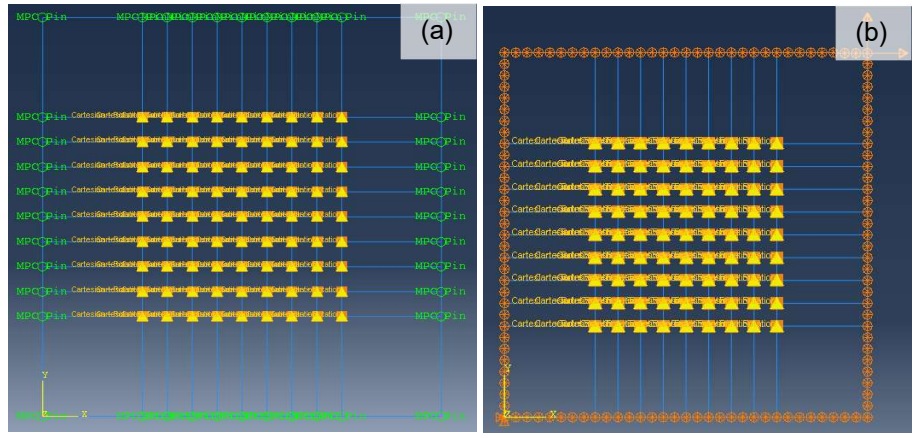


Figure 8. (a) The picture frame test model; (b) the boundary conditions.

To characterize the material and interaction properties, analyses were conducted with and without dashpots. At first, the dashpots were not added, and the material properties and spring stiffness were found by comparing the $F_{normalized}$ vs. γ from experiment and simulation results. It is required that the predicted $F_{normalized}$ at the largest γ (around 55°) should equal to the measured $F_{normalized}$ after relaxation. The dashpot was then added and the coefficient was adjusted until the history of simulated $F_{normalized}$ gets close to that obtained from experiment. The simulation results are shown in Figures 6 and 7. The characterized material and geometric properties are shown in Table II. The stiffness of nonlinear rotational spring k_3 is the slope of the plot of moment along the z-direction M_3 vs. shear angle in the x-y plane γ in Figure 9. A nonlinear damping coefficient for the x-y rotation d_3 is the slope of M_3 vs. shear rate in the x-y plane $\dot{\gamma}$ in Figure 10.

TABLE II. THE CHARACTERIZED PARAMETERS OF THE MODEL.

Parameters	Value	Unit	
а	0.04	mm	
b	4.57	mm kg/mm³ MPa	
ρ	7×10^{-6}		
C_1	60000		
D_1	0	MPa ⁻¹	
y	12	mm	

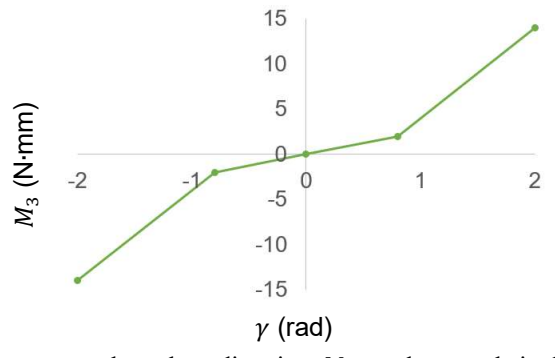


Figure 9. The moment along the z-direction, M_3 vs. shear angle in the x-y plane, γ .

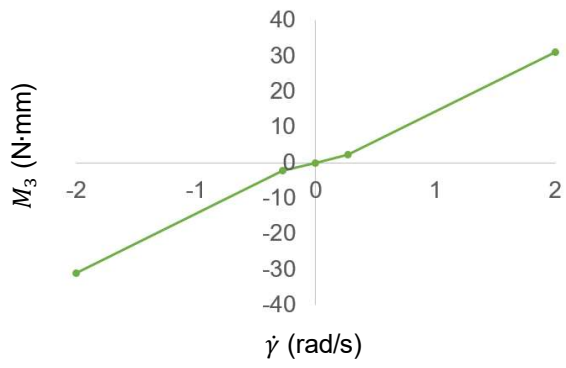


Figure 10. The moment along the z-direction, M_3 vs. shear rate in the x-y plane, $\dot{\gamma}$.

VALIDATION

The proposed model was validated by predicting the fabric deformation during a hemisphere draping test. The shear angles predicted from simulation were compared to those of the deformed fabric measured in the experiment.

Draping experiment

Figure 11 shows the hemisphere draping tool made of an acrylic blank holder, aluminum die support, and steel punch from top to bottom mounted on the MTS load frame. The outer diameter of the punch is 152.4 mm (6"). A hole with a diameter of 160 mm was cut in the center of the die support and blank holder to enable the punch to go though. All the surfaces in contact with fabrics were polished and treated with lubricant to reduce friction.

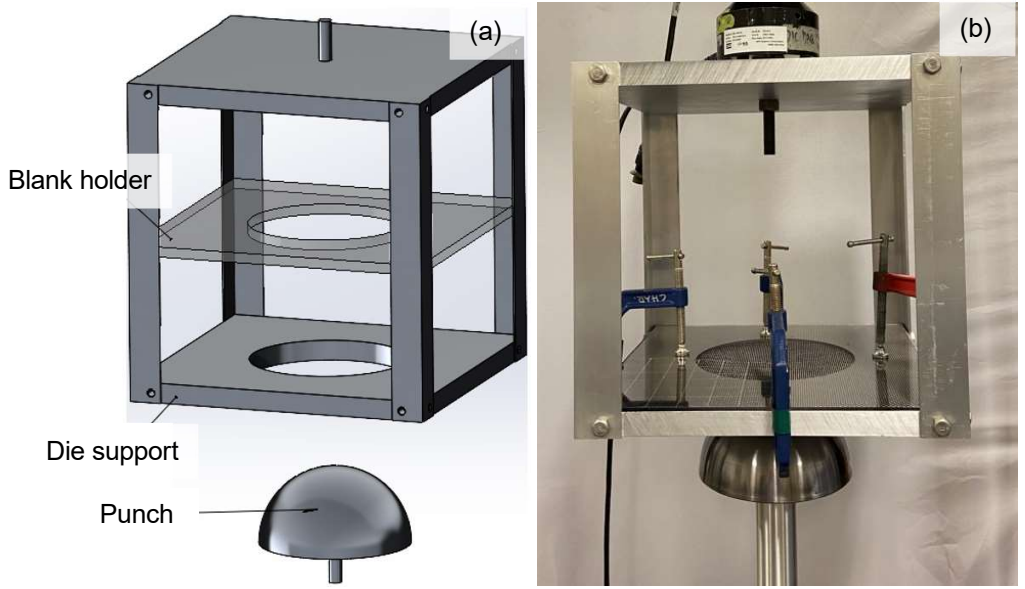


Figure 11. The setup of the hemisphere draping test.

Prior to testing, gridlines were drawn on a piece of T300 carbon fiber reinforced plain-weave fabric ply. The ply was then placed on top of the die support and pressed by the blank holder. To begin with the experiment, the punch was raised to touch the fabric. Then, the fabric was draped upwards for 65 mm in 1 minute. Photos were taken from the top view through the transparent blank holder to record the deformed shape and particularly the shear angle.

The deformed shape is shown in Figure 12. No wrinkle was clearly observed. Fiber sliding slightly happened on the hemisphere. Shear angle tends to be large along diagonal line ($\pm 45^{\circ}$) and it reaches the maximum value near the end of dome. It remains zero at the apex of dome and gradually increases along the diagonal line from apex to the end of the dome. Shear angle decreases as the position moves from the end of dome to the corner of fabric. The angles between the warp and weft tows at five selected points (see Figure 12(b)) are measured and recorded in Table III.

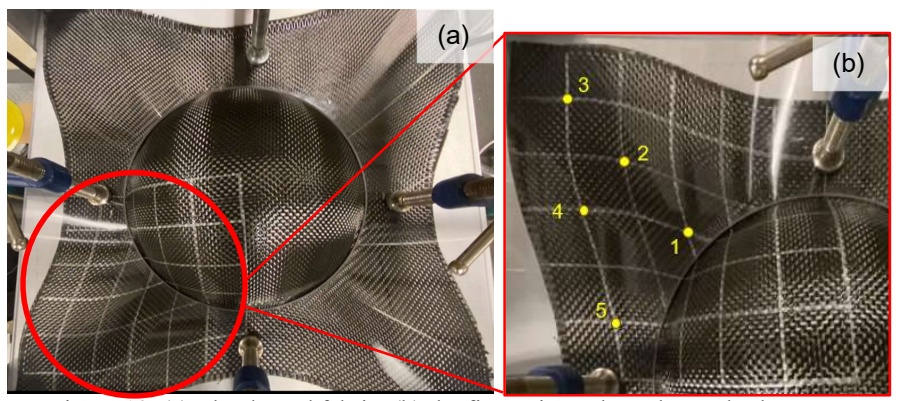


Figure 12. (a) The draped fabric; (b) the five points where the angles between the warp and weft tows are measured.

TABLE III. THE ANGLE BETWEEN THE WEFT AND WARP TOWS FROM THE
EXPERIMENTS AND SIMULATION.

Point	1	2	3	4	5
Experiment	53.6°	71.2°	87.2°	71.4°	74.8°
Simulation $(y = 12 \text{ mm})$	53.1°	76.9°	81.6°	68.1°	72.7°
Simulation $(y = 10 \text{ mm})$	54.4°	75.8°	85.9°	69.6°	74.7°

Draping simulation

A hemisphere draping simulation was conducted for T300 carbon fiber reinforced plain-weave fabric in ABAQUS using dynamic implicit solver. Figure 13 shows the setup. The blank holder, die support and punch were all created as rigid bodies mastered by reference points. Different from the real experiment, the blank holder also pushed towards the fabric when the punch moved along the *z*-direction for 65 mm to solve convergence issue caused by the contact. Only a quarter of fabric was included in the model and symmetric boundary conditions were added at the bottom points (where y=0) and left points (where x=0). Fibers were created as wire parts meshed by 2-node linear

beam elements (B31). The beam section was integrated during the analysis. All the characterized material and geometric properties are summarized in Table II.

Figure 14 (a) shows the deformed shape. Generally, the predicted deformation of the fabric is very similar to the experimental measurement. Similar to the experimental results, the shear angle first increases from the apex to the end of dome and then decreases at the flat region as the position moves along the diagonal of fabric piece. No out-of-plane wrinkle was observed. However, unexpected slight in-plane waviness appears. A possible reason is that the compression of the blank holder creates a compressive axial load, causing slight in-plane buckling. The shear angles were also measured at the same five points and recorded in Table III. It can be concluded that the simulation can accurately predict the shear angle of the deformed fabric by comparing simulation results to experiment results.

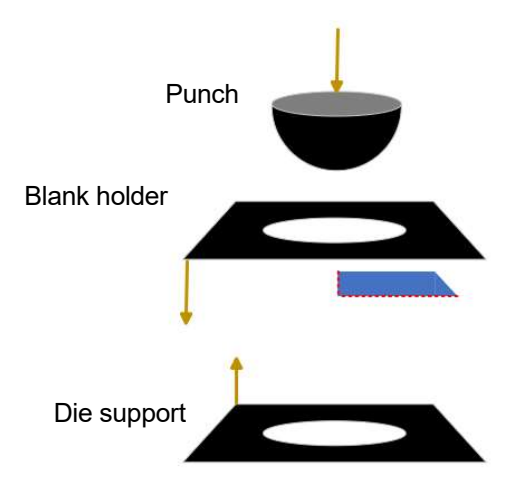


Figure 13. The setup of the hemisphere draping simulation.

In order to show that the yarn spacing is not too large to cause inaccuracy, the characterization and validation were performed again with a yarn spacing of 10 mm, and the predicted draping results are shown in Figure 14 (b). The predicted angles between the warp and weft tows are summarized in Table III. Clearly, the 10 mm case is very close to the 12 mm one. Hence, the value of yarn spacing is appropriate.

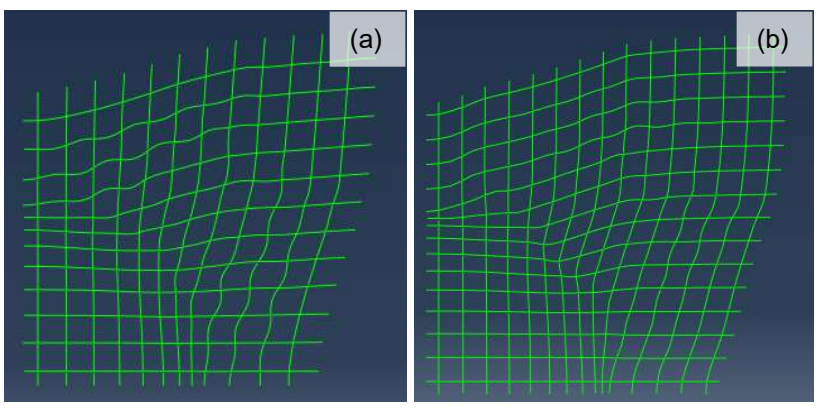


Figure 14. The predicted shape of the hemisphere draping simulation by using (a) y = 12 mm; (b) y = 10 mm.

CONCLUSION

The present paper proposes a modeling methodology for dry fabrics which was modelled as interwoven Timoshenko beam structures connected by springs and dashpots. The bending and in-plane shear properties were characterized by cantilever beam bending test and picture frame test, respectively. The relaxation behavior was successfully captured and characterized by adjusting the damping coefficients. The proposed method was implemented in commercial software Abaqus and applied to simulate the hemisphere draping process. The agreement between deformation of fabric in simulation and that of draped fabric in experiment demonstrates that the model can capture fabric deformation under complex 3-dimensional loading and predict shear angle accurately, even though little in-plane waviness observed in the simulation due to the compaction boundary condition induced by the blank holder. The prediction can be completed efficiently without sacrificing too much accuracy (each job typically finished within 1 hour with only 1 cpu processor). Therefore, the proposed approach can be adopted to simulate fabric draping during LCM and design fabric architecture to achieve target deformation response.

ACKNOWLEDGMENT

The authors are grateful for the support of the National Science Foundation under Grant No. 2105448.

REFERENCES

- [1] Patel, N., and Lee, L. J. "Modeling of Void Formation and Removal in Liquid Composite Molding. Part II: Model Development and Implementation." *Polymer Composites*, Vol. 17, No. 1, 1996, pp. 104–114. https://doi.org/10.1002/pc.10595.
- [2] Olivier, P., Cottu, J. P., and Ferret, B. "Effects of Cure Cycle Pressure and Voids on Some Mechanical Properties of Carbon/Epoxy Laminates." *Composites*, Vol. 26, No. 7, 1995, pp. 509–515. https://doi.org/10.1016/0010-4361(95)96808-J.
- [3] Chung Hae Park, and Woo, L. "Modeling Void Formation and Unsaturated Flow in Liquid Composite Molding Processes: A Survey and Review." *Journal of Reinforced Plastics and Composites*, Vol. 30, No. 11, 2011, pp. 957–977. https://doi.org/10.1177/0731684411411338.
- [4] Rohatgi, V., Patel, N., and Lee, L. J. "Experimental Investigation of Flow-Induced Microvoids during Impregnation of Unidirectional Stitched Fiberglass Mat." *Polymer Composites*, Vol. 17, No. 2, 1996, pp. 161–170. https://doi.org/10.1002/pc.10601.
- [5] Yurgartis, S. W. "Measurement of Small Angle Fiber Misalignments in Continuous Fiber Composites." *Composites Science and Technology*, Vol. 30, No. 4, 1987, pp. 279–293. https://doi.org/10.1016/0266-3538(87)90016-9.
- [6] Khiêm, V. N., Krieger, H., Itskov, M., Gries, T., and Stapleton, S. E. "An Averaging Based Hyperelastic Modeling and Experimental Analysis of Non-Crimp Fabrics." *International Journal of Solids and Structures*, Vol. 154, 2018, pp. 43–54. https://doi.org/10.1016/j.ijsolstr.2016.12.018.
- [7] Hallander, P., Sjölander, J., and Åkermo, M. "Forming Induced Wrinkling of Composite Laminates with Mixed Ply Material Properties; an Experimental Study." *Composites Part A: Applied Science and Manufacturing*, Vol. 78, 2015, pp. 234–245. https://doi.org/10.1016/j.compositesa.2015.08.025.
- [8] Guzman-Maldonado, E., Wang, P., Hamila, N., and Boisse, P. "Experimental and Numerical Analysis of Wrinkling during Forming of Multi-Layered Textile Composites." *Composite Structures*, Vol. 208, 2019, pp. 213–223. https://doi.org/10.1016/j.compstruct.2018.10.018.
- [9] Sjölander, J., Hallander, P., and Åkermo, M. "Forming Induced Wrinkling of Composite Laminates: A Numerical Study on Wrinkling Mechanisms." *Composites Part A: Applied Science*

- *and Manufacturing*, Vol. 81, 2016, pp. 41–51. https://doi.org/10.1016/j.compositesa.2015.10.012.
- [10] Boisse, P., Colmars, J., Hamila, N., Naouar, N., and Steer, Q. "Bending and Wrinkling of Composite Fiber Preforms and Prepregs. A Review and New Developments in the Draping Simulations." *Composites Part B: Engineering*, Vol. 141, 2018, pp. 234–249. https://doi.org/10.1016/j.compositesb.2017.12.061.
- [11] Arnold, S. E., Sutcliffe, M. P. F., and Oram, W. L. A. "Experimental Measurement of Wrinkle Formation during Draping of Non-Crimp Fabric." *Composites Part A: Applied Science and Manufacturing*, Vol. 82, 2016, pp. 159–169. https://doi.org/10.1016/j.compositesa.2015.12.011.
- [12] Takagaki, K., Minakuchi, S., and Takeda, N. "Thick-Walled Crack-Free CFRP Pipes: Stress Reduction Using Atypical Lay-Up." *Composite Structures*, Vol. 126, 2015, pp. 337–346. https://doi.org/10.1016/j.compstruct.2015.02.060.
- [13] Corden, T. J., Jones, I. A., Jones, D. T., and Middleton, V. "The Mechanisms of Interlaminar Cracking in Thick Resin Transfer Moulded Composite Cylinders." *Composites Part A: Applied Science and Manufacturing*, Vol. 29, No. 4, 1998, pp. 455–464. https://doi.org/10.1016/S1359-835X(97)00083-3.
- [14] Albert, C. "Spring-in and Warpage of Angled Composite Laminates." *Composites Science and Technology*, Vol. 62, No. 14, 2002, pp. 1895–1912. https://doi.org/10.1016/S0266-3538(02)00105-7.
- [15] Ali, M., Nawab, Y., Saouab, A., Anjum, A. S., and Zeeshan, M. "Fabrication Induced Spring-Back in Thermosetting Woven Composite Parts with Variable Thickness." *Journal of Industrial Textiles*, Vol. 47, No. 6, 2018, pp. 1291–1304. https://doi.org/10.1177/1528083716686939.
- [16] Hamidi, Y. K., and Altan, M. C. "Process Induced Defects in Liquid Molding Processes of Composites." *International Polymer Processing*, Vol. 32, No. 5, 2017, pp. 527–544. https://doi.org/10.3139/217.3444.
- [17] LI, R., and ZHANG, D. A Fabric Architecture Based Constitutive Model for Fiber Reinforced Rubbers. 2017.
- [18] Li, R., and Zhang, D. "A Textile Architecture-Based Hyperelastic Model for Rubbers Reinforced by Knitted Fabrics." *Acta Mechanica*, Vol. 230, No. 3, 2019, pp. 953–964. https://doi.org/10.1007/s00707-018-2276-2.
- [19] Mathieu, S., Hamila, N., Bouillon, F., and Boisse, P. "Enhanced Modeling of 3D Composite Preform Deformations Taking into Account Local Fiber Bending Stiffness." *Composites Science and Technology*, Vol. 117, 2015, pp. 322–333. https://doi.org/10.1016/j.compscitech.2015.07.005.
- [20] Aimène, Y., Vidal-Sallé, E., Hagège, B., Sidoroff, F., and Boisse, P. "A Hyperelastic Approach for Composite Reinforcement Large Deformation Analysis." *Journal of Composite Materials*, Vol. 44, No. 1, 2010, pp. 5–26. https://doi.org/10.1177/0021998309345348.
- [21] Charmetant, A., Orliac, J. G., Vidal-Sallé, E., and Boisse, P. "Hyperelastic Model for Large Deformation Analyses of 3D Interlock Composite Preforms." *Composites Science and Technology*, Vol. 72, No. 12, 2012, pp. 1352–1360. https://doi.org/10.1016/j.compscitech.2012.05.006.
- [22] Bai, R., Colmars, J., Chen, B., Naouar, N., and Boisse, P. "The Fibrous Shell Approach for the Simulation of Composite Draping with a Relevant Orientation of the Normals." *Composite Structures*, Vol. 285, 2022, p. 115202. https://doi.org/10.1016/j.compstruct.2022.115202.
- [23] Hamila, N., Boisse, P., Sabourin, F., and Brunet, M. "A Semi-Discrete Shell Finite Element for Textile Composite Reinforcement Forming Simulation." *International Journal for Numerical Methods in Engineering*, Vol. 79, No. 12, 2009, pp. 1443–1466. https://doi.org/10.1002/nme.2625.
- [24] Liang, B., Colmars, J., and Boisse, P. "A Shell Formulation for Fibrous Reinforcement Forming Simulations." *Composites Part A: Applied Science and Manufacturing*, Vol. 100, 2017, pp. 81–96. https://doi.org/10.1016/j.compositesa.2017.04.024.
- [25] Wang, Y., and Sun, X. "Digital-Element Simulation of Textile Processes." *Composites Science and Technology*, Vol. 61, No. 2, 2001, pp. 311–319. https://doi.org/10.1016/S0266-3538(00)00223-2.
- [26] Dinh, T., Daelemans, L., and van Paepegem, W. NEAR-MICROSCALE MODELLING OF DRY WOVEN FABRICS UNDER IN-PLANE SHEAR LOADING. 2019.
- [27] Kaka, D., Rongong, J. A., Hodzic, A., and Lord, C. Dynamic Mechanical Properties of Woven Carbon Fibre Reinforced Thermoplastic Composite Materials. 2015.

- [28] Khan, H. A., Hassan, A., Saeed, M. B., Mazhar, F., and Chaudhary, I. A. "Finite Element Analysis of Mechanical Properties of Woven Composites Through a Micromechanics Model." *Science and Engineering of Composite Materials*, Vol. 24, No. 1, 2017, pp. 87–99. https://doi.org/10.1515/secm-2014-0266.
- [29] Lin, H., Clifford, M. J., Long, A. C., and Sherburn, M. "Finite Element Modelling of Fabric Shear." *Modelling and Simulation in Materials Science and Engineering*, Vol. 17, No. 1, 2009, p. 015008. https://doi.org/10.1088/0965-0393/17/1/015008.
- [30] Gatouillat, S., Bareggi, A., Vidal-Sallé, E., and Boisse, P. "Meso Modelling for Composite Preform Shaping Simulation of the Loss of Cohesion of the Woven Fibre Network." *Composites Part A: Applied Science and Manufacturing*, Vol. 54, 2013, pp. 135–144. https://doi.org/10.1016/j.compositesa.2013.07.010.
- [31] Faccio Júnior, C. J., and Gay Neto, A. "Challenges in Representing the Biaxial Mechanical Behavior of Woven Fabrics Modeled by Beam Finite Elements with Contact." *Composite Structures*, Vol. 257, 2021, p. 113330. https://doi.org/10.1016/j.compstruct.2020.113330.
- [32] Saito, M., and Neto, A. Woven Fabrics Computational Simulation Using Beam-to-Beam Contacts Formulation. 2016.
- [33] Harrison, P. "Modelling the Forming Mechanics of Engineering Fabrics Using a Mutually Constrained Pantographic Beam and Membrane Mesh." *Composites Part A: Applied Science and Manufacturing*, Vol. 81, 2016, pp. 145–157. https://doi.org/10.1016/j.compositesa.2015.11.005.
- [34] Sun, H., and Pan, N. "Shear Deformation Analysis for Woven Fabrics." *Composite Structures*, Vol. 67, No. 3, 2005, pp. 317–322. https://doi.org/10.1016/j.compstruct.2004.01.013.
- [35] Taha, I., Abdin, Y., and Ebeid, S. "Comparison of Picture Frame and Bias-Extension Tests for the Characterization of Shear Behaviour in Natural Fibre Woven Fabrics." *Fibers and Polymers*, Vol. 14, No. 2, 2013, pp. 338–344. https://doi.org/10.1007/s12221-013-0338-6.
- [36] Shen, H., Wang, P., and Legrand, X. "In-Plane Shear Characteristics during the Forming of Tufted Carbon Woven Fabrics." *Composites Part A: Applied Science and Manufacturing*, Vol. 141, 2021, p. 106196. https://doi.org/10.1016/j.compositesa.2020.106196.
- [37] Lindberg, J., Behre, B., and Dahlberg, B. "Part III: Shearing and Buckling of Various Commercial Fabrics." *Textile Research Journal*, Vol. 31, No. 2, 1961, pp. 99–122. https://doi.org/10.1177/004051756103100203.
- [38] Dinh, T., Daelemans, L., and van Paepegem, W. Near-Microscale Modelling of Dry Woven Fabrics under in-Plane Shear Loading. 2019.
- [39] Wang, Y., Zhang, W., Ren, H., Huang, Z., Geng, F., Li, Y., and Zhu, Z. "An Analytical Model for the Tension-Shear Coupling of Woven Fabrics with Different Weave Patterns under Large Shear Deformation." *Applied Sciences*, Vol. 10, No. 4, 2020, p. 1551. https://doi.org/10.3390/app10041551.
- [40] Mohammed, U., Lekakou, C., Dong, L., and Bader, M. G. "Shear Deformation and Micromechanics of Woven Fabrics." *Composites Part A: Applied Science and Manufacturing*, Vol. 31, No. 4, 2000, pp. 299–308. https://doi.org/10.1016/S1359-835X(99)00081-0.
- [41] Habboush, A., Sanbhal, N., Shao, H., Jiang, J., and Chen, N. "Characterization and Analysis of In-Plane Shear Behavior of Glass Warp-Knitted Non-Crimp Fabrics Based on Picture Frame Method." *Materials*, Vol. 11, No. 9, 2018, p. 1550. https://doi.org/10.3390/ma11091550.
- [42] Cao, J., Akkerman, R., Boisse, P., Chen, J., Cheng, H. S., de Graaf, E. F., Gorczyca, J. L., Harrison, P., Hivet, G., Launay, J., Lee, W., Liu, L., Lomov, S. V., Long, A., de Luycker, E., Morestin, F., Padvoiskis, J., Peng, X. Q., Sherwood, J., Stoilova, Tz., Tao, X. M., Verpoest, I., Willems, A., Wiggers, J., Yu, T. X., and Zhu, B. "Characterization of Mechanical Behavior of Woven Fabrics: Experimental Methods and Benchmark Results." Composites Part A: Applied 2008, and Manufacturing, Vol. No. 6, pp. 1037–1053. Science 39, https://doi.org/10.1016/j.compositesa.2008.02.016.
- [43] Boisse, P., Hamila, N., Guzman-Maldonado, E., Madeo, A., Hivet, G., and dell'Isola, F. "The Bias-Extension Test for the Analysis of in-Plane Shear Properties of Textile Composite Reinforcements and Prepregs: A Review." *International Journal of Material Forming*, Vol. 10, No. 4, 2017, pp. 473–492. https://doi.org/10.1007/s12289-016-1294-7.
- [44] Peng, X. Q., Cao, J., Chen, J., Xue, P., Lussier, D. S., and Liu, L. "Experimental and Numerical Analysis on Normalization of Picture Frame Tests for Composite Materials." *Composites Science and Technology*, Vol. 64, No. 1, 2004, pp. 11–21. https://doi.org/10.1016/S0266-3538(03)00202-1.